The light curve of the companion to PSR J2051-0827

Stappers, B.W.; van Kerkwijk, M.H.; Lane, B.; Kulkarni, S.

Published in:
Astrophysical Journal

DOI:
10.1086/311795

THE ASTROPHYSICAL JOURNAL, 510:L45–L48, 1999 January 1

THE LIGHT CURVE OF THE COMPANION TO PSR J2051−0827

B. W. STAPPERS,[1,2] M. H. VAN KERKWIJK,[3,4,5] B. LANE,[4] AND S. R. KULKARNI[4]

Received 1998 September 4; accepted 1998 November 2; published 1998 December 1

ABSTRACT

We have obtained new photometry of the companion to the eclipsing binary millisecond pulsar PSR J2051−0827. The data are modeled by a gravitationally distorted, low-mass secondary star that is irradiated by the impinging pulsar wind. The best-fit models require that greater than 30% of the incident energy is absorbed by the secondary star and reradiated as optical emission. Unless the companion is significantly farther away than its dispersion measure distance, it underfills its Roche lobe by at least 30%. A small companion makes it difficult to drive a wind from its surface and thus explain the mass loss in the system. Our models show that the system is inclined by more than 30°, and thus the companion mass is in the range of 0.025–0.055 $M_\odot$ (for a 1.4 $M_\odot$ pulsar). The unilluminated side of the companion is cool, with a best-fit temperature of 3000 K.

Subject headings: binaries: eclipsing — pulsars: individual (PSR J2051−0827) — stars: neutron

1. INTRODUCTION

The PSR J2051−0827 binary system is only the second for which heating effects of the pulsar's relativistic wind on the companion have been observed (Stappers, Bessell, & Bailes 1996b). Optical observations indicate that the companion's brightness varies by more than 1.2 mag in *R* as its heated side rotates in and out of view. The pulsed radiation from the 4.5 ms pulsar is eclipsed for approximately 10% of the 2.4 hr orbital period, indicating that there must be material extending beyond the Roche lobe of the companion (Stappers et al. 1996a).

PSR J2051−0827 joins PSR B1957+20 and PSR B1744−24A as systems that are believed to be in the process of ablating their companions and becoming isolated millisecond pulsars (Fruchter, Stinebring, & Taylor 1988; Lyne et al. 1990). The existence of these systems provides a vital clue to understanding whether (and, if so, how) isolated millisecond pulsars can be the descendants of low-mass X-ray binaries (see, e.g., Bhattacharya & van den Heuvel 1991). There are two broad methods by which the companions in these system may be destroyed: either ablation by the pulsar's relativistic wind or tidal dissipation through Roche lobe overflow. The former has been the most popular, but whether it can work is not clear and is highly dependent on the pulsar's energetics (see, e.g., Levinson & Eichler 1991). The low spin-down energy impinging on the companion of PSR J2051−0827 makes it difficult to remove sufficient material. Indeed, the low-electron column density at the eclipse boundaries indicates that there is only a small amount of ionized material present. However, a Roche lobe filling companion greatly facilitates the mass-loss process since much less energy is required to drive a wind from its surface, and mass may also be lost through the inner Lagrangian point (Fruchter & Goss 1992; Banit & Shaham 1992). For PSR B1957+20, it may also help to explain the variable orbital period derivative (Arzoumanian, Fruchter, & Taylor 1994; Applegate & Shaham 1994).

The revision of the distance estimate to PSR B1957+20 means the companion's radius is now consistent with it filling its Roche lobe (Fruchter & Goss 1992). Modeling has shown that a quite highly irradiated secondary, which is close to filling its Roche lobe, can successfully fit the orbital light curve of PSR B1957+20 (Callanan, van Paradijs, & Regelink 1995; van Kerkwijk et al. 1999).

We have carried out further photometry of the companion to PSR J2051−0827 and have detected it over a larger range of binary phase than in previous observations (Stappers et al. 1996b). This improved orbital coverage allows us to model the light curve by emission from a tidally distorted star heated by the impinging radiation from the pulsar.

2. OBSERVATIONS

PSR J2051−0827 was observed for us by S. Djorgovski and M. Pahre on the night of 1995 September 19 using the Palomar Mountain 200 inch (5 m) telescope. Images were obtained using a Tek 2048 CCD detector at prime focus, with an effective pixel size of 0″.28 and a field of view of 9′.7 × 9′.7. The seeing was typically 0″.9. A total of 22 consecutive images were taken in Gunn *i* with an integration time of 300 s, and the whole 2.4 hr binary period was covered. The weather was not photometric for these observations. To enable proper calibration, further observations of the pulsar's field and of the standard field Mark A (Landolt 1992) were made in photometric conditions on 1996 October 21. IRAF was used to debias and flat-field the images, using both dome and night-sky flats. Since the field near the optical companion is not crowded, instrumental Gunn *i* magnitudes were calculated using the IRAF aperture photometry task. Bright stars with well-defined point-spread functions were used to calculate aperture corrections.

Observations of the standard field were reduced using a similar procedure, and they were used to calculate the transformation between the instrumental Gunn *i* magnitudes and the calibrated Cousins *I* magnitudes. There is no color term in the transformation since the standard deviation is just 0.007 mag for standard stars with $V - I$ colors ranging from −0.237 to 1.092. A comparison of the spectral response curve for the combined CCD and Gunn *i* system with that for *I* confirms the small color term (M. S. Bessell 1997, private communication). Ten stars that did not vary significantly between the two ob-

[1] Sterrenkundig Instituut "Anton Pannekoek," Universiteit van Amsterdam, Kruislaan 403, 1098 SJ Amsterdam, The Netherlands.

[2] Mount Stromlo and Siding Spring Observatories, Institute of Advanced Studies, Australian National University, Private Bag, Weston Creek Post Office, ACT 2611, Australia.

[3] Institute of Astronomy, University of Cambridge, Madingley Road, Cambridge, CB3 0HA, England, UK.

[4] California Institute of Technology, MS 105-24, Pasadena, CA 91125.

[5] Present address: Sterrekundig Instituut, University of Utrecht, P.O. Box 80000, 3508 TA Utrecht, The Netherlands.

TABLE 1

I AND *R* MAGNITUDES USED IN THE LIGHT CURVE FITTING

Phase	Band	Magnitude	Error
	Palomar		
0.238	*I*	23.05	0.25
0.291	*I*	22.48	0.14
0.344	*I*	22.16	0.11
0.397	*I*	22.04	0.09
0.450	*I*	21.87	0.08
0.503	*I*	21.85	0.08
0.556	*I*	21.84	0.08
0.609	*I*	21.90	0.09
0.662	*I*	22.06	0.10
0.715	*I*	22.70	0.20
0.768	*I*	22.64	0.17
0.814	*I*	23.08	0.25
0.822	*I*	22.90	0.20
	Anglo-Australian Telescope[a]		
0.689	*I*	22.37	0.14
0.797	*I*	23.19	0.30
0.314	*R*	23.10	0.10
0.402	*R*	22.62	0.08
0.510	*R*	22.34	0.06
0.617	*R*	22.71	0.07
0.725	*R*	23.24	0.13

[a] Magnitudes are from Stappers et al. 1996b.

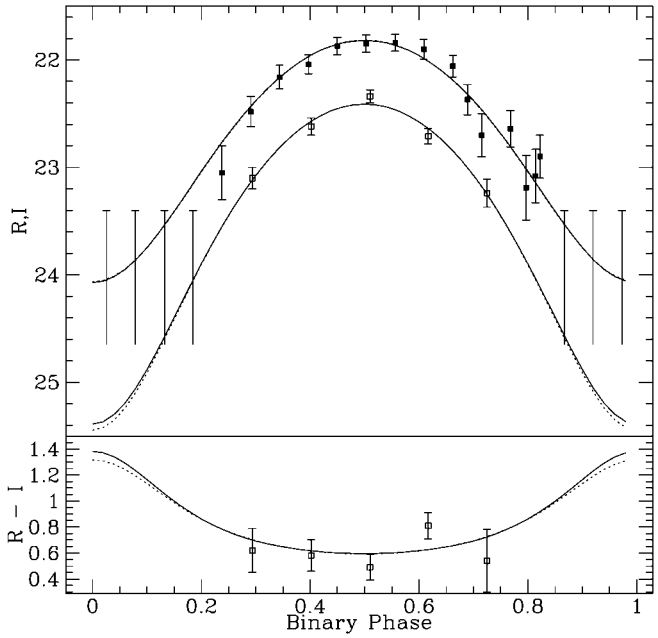

FIG. 1.—The $R-I$ color variation and R (*lower*) and I (*upper*) light curves from the best-fit models (see Table 2) for both the solar (*solid line*) and the one-tenth solar (*dotted line*) metallicity are compared with the data from Table 1. The $R-I$ color variation is derived from the I and R fits, and the $R-I$ data points are derived from R and I observations at approximately the same phase.

serving epochs, with colors for which our transformation was valid, were used to define the frame-to-frame baseline. The total calibration error is ∼0.04 mag. The resulting I magnitudes were compared with those obtained by Stappers et al. (1996b), and are consistent within the errors.

Observations were also made in J and K using the Cassegrain IR camera on the Palomar Mountain 200 inch (5 m) telescope. The total field of view is 37″.0 × 35″.0, with an effective pixel size of 0″.165, and the seeing was ∼0″.9. Again, IRAF was used to debias, flat-field, and combine the data. Approximately a full orbit was covered in both bands. The companion was not seen at any phase, and therefore the observations were combined to generate upper limits of ∼22.0 and ∼21.0 in J and K, respectively.

The I magnitudes presented here (Palomar) and the R and I data from Stappers et al. (1996a) (Anglo-Australian Telescope) are listed in Table 1. Note that for the binary phase, ϕ, we use a different convention, in which the pulsar is eclipsed at $\phi = 0.0$ (cf. $\phi = 0.25$) and the companion magnitude is greatest at $\phi = 0.5$ (cf. $\phi = 0.75$). A slight asymmetry is apparent in the shape of the I light curve (see Fig. 1). However, we caution that this may be due to a few minutes offset in the clock of the data acquisition system. This offset will not alter the conclusions we draw.

3. MODEL

The R and I light curves were fitted with a model of an irradiated companion developed by one of us (M. H. v. K.). This model follows the prescriptions of Tjemkes, van Paradijs, & Zuiderwijk (1986) and is discussed in more detail in van Kerkwijk et al. (1999). Irradiation, tidal and rotational distortion of the companion, and gravity darkening (von Zeipel 1924) are considered.

The I upper limits in the nondetection frames are all 23.4. Only the upper limits at phases most immediately before and after a detection were used in the fits. The magnitudes were defined such that the upper limit of the 3 σ error bar corresponded to the 3 σ detection limit. The quality of the fit was not greatly altered by considering different errors, but the exclusion of these upper limits reduced the constraints that could be placed on the fitted parameters.

Since the unirradiated side of the companion star is likely very cool, the emergent spectrum needs to be modeled carefully. We used an updated version of the stellar atmosphere models of Allard & Hausschildt (1995) to calculate the emergent flux at different points on the surface. The companion's metallicity is unknown; therefore, we tried models with both solar and one-tenth solar metallicity. The models spanned effective temperatures $T_{\rm eff} = 2000, 2200, \ldots, 7000$ K and specific gravities $\log g = 3.5, 4.0, 4.5, 5.0$. They consist of specific intensities for 16 direction cosines in 5 Å bins between 0.3 and 3 μm. The specific intensities were integrated over the filter bandpasses given by Bessell (1990) and Bessell & Brett (1988).

Nine parameters can be varied during the fitting process: distance modulus (ΔM), J-band extinction (A_J), orbital inclination (i), corotation factor ($f_{\rm co}$, the ratio of the rotational and orbital frequency of the companion), filling factor (β, ratio of the stellar and Roche radii), irradiation efficiency (η, fraction of incident pulsar spin-down energy absorbed and reradiated by the companion), back-side temperature (T_B, temperature of the unilluminated face of the companion, as measured at the pole), gravity darkening exponent (α), and pulsar mass ($M_{\rm PSR}$). The I and R data are fitted simultaneously. The fit was insensitive to $f_{\rm co}$ and $M_{\rm PSR}$, and so these are taken to be 1 and 1.4 $M_\odot$, respectively. Gravity darkening is assumed to cause variations in the temperature prescribed by $T \propto g^\alpha$. We used $\alpha = 0.08$, which is appropriate for a convective atmosphere (Lucy 1967).

Holding α, $M_{\rm PSR}$, and $f_{\rm co}$ fixed leaves six variable parameters. Inclinations between 30° and 90° were considered, and for each value, the projected semimajor axis and the mass function were used to recalculate the secondary mass and Roche lobe radius.

TABLE 2
BEST-FIT MODEL

PARAMETER	METALLICITY	
	Solar	One-Tenth Solar
Metallicity (fixed)	0.0	−1.0
Distance modulus	10.84	10.93
J-band extinction	0.052	0.056
χ^2 (16 dof)	16.6	16.6
Inclination (deg)	37	40
Filling factor	0.51	0.53
Irradiation efficiency	0.42	0.42
Temperature (K)	2717	2581
Companion radius ($R_\odot$)	0.075	0.078

Inclination angles less than 30° required $T_B < 2000$ K. Such T_B were not considered since they reach the limits of the atmospheric models. Fits where $\beta < 0.2$ were also not considered since they required specific gravities that were too large.

4. RESULTS

Parameters from the best-fit models for the two metallicities are listed in Table 2. They indicate that the system is mildly inclined and the companion is only half filling its Roche lobe. A large fraction of the pulsar spin-down energy, 42%, is required to power the heating of the companion. The fitted value for A_J is small, which is consistent with the low reddening expected in the direction of the system (Stappers et al. 1996b). However, there is a large range of valid solutions. Figure 2 shows χ^2 contours for two pairs of parameters. These were generated by stepping through a grid of values for each pair and refitting for the remaining variable parameters.

In the left-hand panels of Figure 2, χ^2 is shown as a function of η and β (*solid contours*). Lines of constant ΔM (*dotted contours*) and A_J (*dashed contours*) are also shown. A strong lower limit on η is apparent. At maximum, the light is dominated by reprocessed radiation, and the minimum efficiency reflects the well-constrained color temperature. No strong upper limit exists because the model can compensate for the increasing blueness of a highly irradiated star by increasing the interstellar reddening (the role of reddening will be discussed in more detail below). The largest possible β-values are ruled out by the shape of the light curve. If the companion is too close to filling its Roche lobe, then, as we move away from maximum, its magnitude does not fall off sufficiently quickly to match the data. In fact, our current data show no evidence of deformation of the companion star, only of irradiation. This accounts for the interdependence between the distance to the system and β.

The variation of χ^2 with T_B and i (*right-hand panels*) shows that they are correlated. When i is decreased, the modulation decreases too, and to bring it in line with the observations again, either η has to be increased or T_B decreased. At the same time, the variation in color temperature as well as, perhaps more importantly, the light-curve shape has to be maintained. The latter may not be immediately obvious, since it might appear that a change in η can always compensate for a change in temperature (with interstellar reddening compensating for the associated change in color). Indeed, if one varies η proportionally to T_B^4, the relative temperature distribution over the surface does not change. However, the temperature dependence of the flux in a given band will change, and hence the relative surface brightness distribution in that band will change, as will

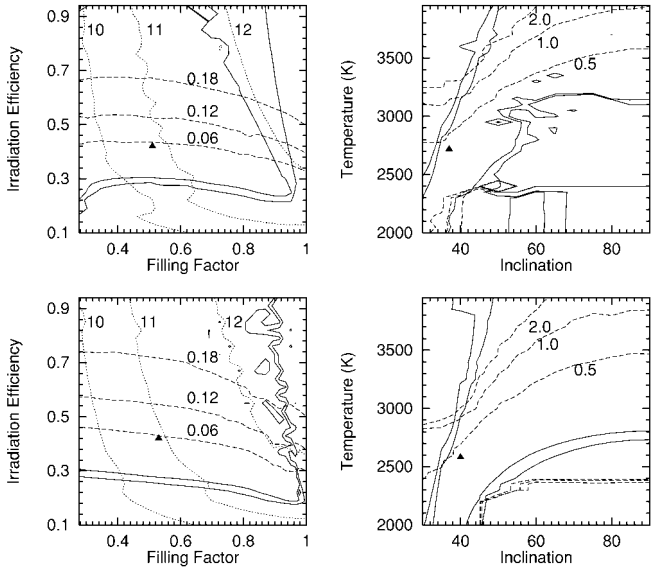

FIG. 2.—Comparison of the χ^2 contours ($\chi^2_{\rm min} + 1$, $\chi^2_{\rm min} + 2$) for filling factor vs. irradiation efficiency and temperature vs. inclination. Both the solar (*top panels*) and the one-tenth solar (*bottom panels*) metallicity are shown. The dotted contours correspond to constant ΔM in the irradiation plots. The dashed contours correspond to constant A_J and η in the irradiation and temperature plots, respectively. These secondary contours have values as labeled. The best-fit values are indicated by the filled triangles.

the shape of the light curve.[6] At high temperature, the *I* brightness dependence on temperature is weak, and at low *i*, the drop-off around maximum is slower than observed (and, less importantly, the $R - I$ color changes too slowly). Conversely, at low temperature and high *i*, the variation is more rapid.

In summary, based on modeling of the light curve, we can only set a lower limit on η. However, we have additional information that enables us to constrain the reddening and the distance. As discussed by Stappers et al. (1996b), PSR J2051−0827 lies well below the Galactic plane, and the reddening is low. They derived $E(B - V) \approx 0.03$–0.06 from the reddening maps of Burstein & Heiles (1982). These maps show the total Galactic reddening, are based on galaxy counts and H I column densities, and have a quoted uncertainty of only 0.01 mag. Another method of determining reddening uses *IRAS* 100 μm measurements (Laureijs, Helou, & Clark 1994). At the position of the pulsar, we find a surface brightness of 2.5 MJy sr^{-1} corresponding to $A_B \approx 0.3$, and thus $E(B - V) \approx 0.07$. It is also possible to use the pulsar's dispersion measure to constrain the distance, 1.3 kpc (Taylor & Cordes 1993), and thus the radius of the companion, 0.07 $R_\odot$, which corresponds to $\eta \sim 0.5$. The 1 σ error in the distance, and thus also in the radius, is $\pm 30\%$.

We remodeled the data with the additional constraints, $\Delta M = 10.6 \pm 0.6$ and $A_J = 0.06 \pm 0.03$. The results (Fig. 3) show that the model parameters are indeed much better constrained. The lower bound on η (30%) is unaffected, as expected, while the upper limit (70%) is determined by the constraint on the reddening. The aforementioned correlation between the companion radius, with no deformation, and the distance is further highlighted here, with the contours running almost parallel to the lines of constant distance. A comparison

[6] The shape will not change if the band is in the Rayleigh-Jeans tail for all temperatures considered. The bolometric light curve will not change either.

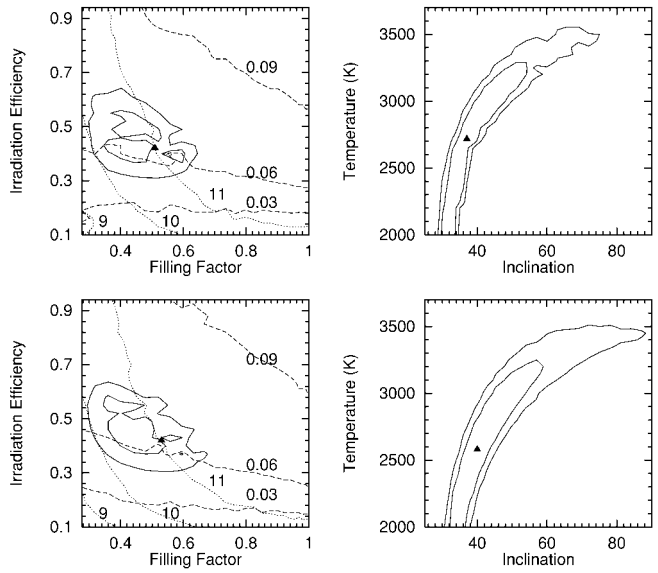

FIG. 3.—Comparison of the χ^2 contours ($\chi^2_{\rm min}+1$, $\chi^2_{\rm min}+2$) for filling factor vs. irradiation efficiency and temperature vs. inclination for fits where the reddening and the distance were constrained as described in the text. Both the solar (*top panels*) and the one-tenth solar (*bottom panels*) metallicity are shown. Additional contours in the irradiation efficiency plots and filled triangles are the same as for Fig. 2.

of T_B and i in Figure 3 elucidates their strong interdependence. The lower limit on i is much stronger; even for the coolest companion that we were able to model, i will not be less than 30°.

Differences between the metallicities in all fits are not great. Where they do differ, T_B is most predominantly affected; i.e., where the temperature of the companion is coolest, the effects of different metallicity will be most evident in the emergent spectrum. The model estimates for the J and K fluxes are less than our nondetection limits. A prediction of our best-fit model for the shape of the J light curve indicates that the variation between the two metallicities is slightly greater in this band.

5. DISCUSSION

From our models, we find a strong lower constraint on the efficiency for the reprocessing of the impinging pulsar flux to optical light. The spin-down energy of PSR J2051−0827 is $4\pi^2 I(P/P^3) \approx 5.7 \times 10^{33}$ ergs s^{-1}, for a moment of inertia, $I = 10^{45}$ g cm^{-2}, pulse period, P, and period derivative, P. Between 30% and 70% of this energy is required to power the optical emission. Thus, little remains to drive a wind from the companion. This efficiency is larger than that found for PSR B1957+20 by Callanan et al. (1995).

The companion to PSR J2051−0827 lies well inside its Roche lobe, unless the distance to the system is significantly greater than 2 kpc. Such underfilling of the Roche lobe, combined with the large amount of energy required to power the optical emission, makes it difficult to explain the mass loss that appears to be occurring in the system. A large range of backside temperatures are possible, but probably it will be less than ~3000 K, which is similar to what was found for the companion to PSR B1957+20 (Fruchter, Bookbinder, & Bailyn 1995). The inclination is most likely greater than ~30°. The corresponding maximum companion mass is 0.055 $M_\odot$ (for a 1.4 $M_\odot$ neutron star).

The best-fit models presented here predict that the unilluminated side of the companion should have magnitudes $R < 25.4$ and $I < 24$ at minimum. Detection of the companion at minimum light is required to constrain further both the unilluminated companion temperature and the geometry of the system. It may also help us to place constraints on the composition of the companion star.

We thank Mike Pahre for his helpful advice on data reduction procedures and Paul Groot and Titus Galama for suggesting the use of the *IRAS* for reddening estimates. B. W. S. acknowledges support from the ANU, M. H. v. K. from NASA through a Hubble fellowship, and S. R. K. from NASA and the NSF.

REFERENCES

Allard, F., & Hauschildt, P. H. 1995, ApJ, 445, 433
Applegate, J. H., & Shaham, J. 1994, ApJ, 436, 312
Arzoumanian, Z., Fruchter, A. S., & Taylor, J. H. 1994, ApJ, 426, L85
Banit, M., & Shaham, J. 1992, ApJ, 388, L19
Bessell, M. S. 1990, PASP, 102, 1181
Bessell, M. S., & Brett, J. M. 1988, PASP, 100, 1134
Bhattacharya, D., & van den Heuvel, E. P. J. 1991, Phys. Rep., 203, 1
Burstein, D., & Heiles, C. 1982, AJ, 87, 1165
Callanan, P. J., van Paradijs, J., & Regelink, R. 1995, ApJ, 439, 928
Fruchter, A. S., Bookbinder, J., & Bailyn, C. 1995, ApJ, 443, L21
Fruchter, A. S., & Goss, W. M. 1992, ApJ, 384, L47
Fruchter, A. S., Stinebring, D. R., & Taylor, J. H. 1988, Nature, 333, 237
Landolt, A. U. 1992, AJ, 104, 372
Laureijs, R. J., Helou, G., & Clark, F. O. 1994, in ASP Conf. Ser. 58, The First Symposium on the Infrared Cirrus and Diffuse Interstellar Clouds, ed. R. M. Cutri & W. B. Latter (San Francisco: ASP), 133
Levinson, A., & Eichler, D. 1991, ApJ, 379, 359
Lucy, L. 1967, Z. Astrophys., 65, 89
Lyne, A. G., et al. 1990, Nature, 347, 650
Stappers, B. W., et al. 1996a, ApJ, 465, L119
Stappers, B. W., Bessell, M. S., & Bailes, M. 1996b, ApJ, 473, L119
Taylor, J. H., & Cordes, J. M. 1993, ApJ, 411, 674
Tjemkes, S. A., & van Paradijs, J., & Zuiderwijk, E. J. 1986, A&A, 154, 77
van Kerkwijk, M. H., Lane, B., Kulkarni, S. R., & Stappers, B. W. 1999, in preparation
von Zeipel, H. 1924, MNRAS, 84, 665